VALIDATION OF THE OPERATIONAL MERIS FAPAR PRODUCTS

Nadine Gobron [(1)], Ophélie Aussedat [(1)], Thomas Lavergne [(1)], Malcolm Taberner [(1)], Bernard Pinty [(1)], Fabrice Brito [(2)], Olga Faber [(3)], Carsten Brockmann [(3)], Frédéric Mélin [(1)], Monica Robustelli [(1)] and Paul Snoeij [(4)]

[(1)]European Commission – DG Joint Research Centre, Institute for Environment and Sustainability, Global Environment Monitoring Unit, TP 440, via E. Fermi, 21020 Ispra (VA), Italy, Email: nadine.gobron@jrc.it
[(2)]European Space Agency, European Space Research INstitute, via Galileo Galilei, 00044 Frascati (RM), Italy
[(3)]Carsten Brockmann Consult, Ottilie-Baader-Str. 15 21035 Hamburg, Germany
[(4)]European Space Agency EOP-SMS European Space Research and Technology Centre -, Keplerlaan 1, P.O. Box 299, 2200 AG Noordwijk, The Netherlands

ABSTRACT

This contribution discusses the validation of the operational Medium Resolution Imaging Spectrometer (MERIS) Level 2 land product which corresponds to the biophysical variable of the Fraction of Absorbed Photosynthetically Active Radiation (FAPAR). The FAPAR value acts as an indicator of the presence and state of the vegetation and it can be estimated from MERIS data at both reduce and full resolution using a physically-based approach. The quality of the MERIS FAPAR products, derived from the MERIS Global Vegetation Index (MGVI) algorithm, capitalizes on the availability of three years of MERIS data over the full globe.

The validation exercises proposed here assess the accuracy and the quality of the MGVI product by 1) analyzing the estimates of theoretical FAPAR uncertainties (versus the algorithm formulae and instrument calibration performance), 2) comparing MGVI values to similar products generated by other independent sensors like the Sea-viewing Wide Field-of-view Sensor (SeaWiFS) and the MODerate Resolution Imaging Spectro-radiometer (MODIS) with either co-located and quasi simultaneously acquired data or over the same regional area with temporally composited products, and finally 3) comparing these remote sensing products against ground-estimates of FAPAR which have been performed over specific types of land cover during one seasonal cycle.

1. Introduction

The MGVI algorithm was developed to produce useful, quantitative, reliable and accurate information on the state of terrestrial vegetation using MERIS Level 1 data, *i.e.* Top Of Atmosphere (TOA) Bidirectional Reflectance Factors (BRFs). The operational constraints were to deliver a computationally efficient algorithm for documenting surface biophysical activity, applicable to every single acquisition date at any resolution over any land surface and vegetation type ([[1] and [2]). The algorithm's data inputs are the calibrated MERIS L1 data in the blue (442 nm), red (680 nm) and near-infrared (865 nm) bands as well as the illumination and observation angles. The methodology adopted to design this algorithm relies on physically-based radiative transfer models to limit the angular, atmospheric and soil background contamination effects. It first requires the design of an extensive set of geophysical scenarios of sensor-like data representing various land surface conditions. This data set, used as a training data set for the algorithm optimization and, in the first section for the evaluation of the theoretical uncertainties, has been established on the basis of surface radiation transfer models coupled with atmospheric models. This approach yields a large number of simulated radiance fields, which can then be sampled by a virtual instrument similar to the actual one in terms of the spectral and angular observation sampling schemes. The corresponding FAPAR values for the various simulated terrestrial systems are estimated simultaneously as part of the radiation transfer model outputs. More specifically, simulations are conducted with a plane-parallel structurally homogeneous canopy model [3] representing the land component; it is coupled with the Second Simulation of the Satellite Signal in the Solar Spectrum (6S) model [4] in order to represent the atmospheric effects. Since green vegetation strongly absorbs solar radiation in the red spectral region, and strongly scatters it in the near-infrared, these two bands are widely used to characterize land surfaces from remote sensing data. The reflectance in the blue band is sensitive to the aerosol optical thickness and is therefore used to decontaminate the red and the near-infrared bands from atmospheric effects. The decontamination from directional effects is achieved using a parametric angular model [5]. The design of the FAPAR algorithm, here the MGVI, is based on a two steps procedure where the spectral reflectances measured in the red and near-infrared bands are, first rectified in order to ensure their 'decontamination' from atmospheric and angular effects and, second combined together in a mathematical formula to generate the FAPAR value. Similar FAPAR algorithms have been developed for various optical sensors [6] and to provide an accuracy of about ± 0.1 on average for the daily

FAPAR values. The last updated version for MERIS can be found in [7].
The validation exercises proposed here aim at assessing both the accuracy and the quality of the MGVI product in three phases.
In the first section, the theoretical accuracies due to the input data quality are first derived by estimates of FAPAR uncertainties using the algorithm formulae itself and instrument calibration information. We also show the expected differences between the FAPAR products derived from two sensors as function of their "inter-calibration" agreement.
The second section summarizes the results of comparisons between MGVI values and similar products generated by other independent sensors like SeaWiFS and MODIS over one example of co-located and quasi simultaneously acquired data, as well as using higher level product, i.e. time composite products over Europe.
The third part shows time series of comparison between FAPAR derived from three sensors against ground-estimates of FAPAR which has been made over one type of land cover during one seasonal cycle. This last phase was derived from a careful analysis of the problem which ended up in the grouping of available field information into broad categories representing different radiative transfer regimes [8]. This greatly helps the interpretation of the results since it recognizes the various level of difficulties and sources of uncertainties associated with the radiative sampling of different types of vegetation canopies.

2. Assessment of the accuracies from FAPAR formulae using data inputs uncertainties

The MERIS FAPAR products are computed from the three spectral bands in the blue, red and near-infrared domains. The FAPAR uncertainty can be therefore assessed by deriving the algorithm formulae with respect to these reflectances as is expressed by Eq. 1.

$$\Delta FAPAR = \frac{\partial FAPAR}{\partial \rho_{BLUE}}\Delta\rho_{BLUE} + \frac{\partial FAPAR}{\partial \rho_{RED}}\Delta\rho_{RED} + \frac{\partial FAPAR}{\partial \rho_{NIR}}\Delta\rho_{NIR} \quad (1)$$

where $\Delta\rho_\lambda$ is the relative accuracy of radiances at the top of the atmosphere for each band λ.
Eq. (1) can be re-written as follows:

$$\Delta FAPAR = \frac{\partial g_0}{\partial \rho_{RectRED}}\Delta\rho_{RectRED} + \frac{\partial g_o}{\partial \rho_{RectNIR}}\Delta\rho_{RectNIR} \quad (2)$$

where the uncertainties in the red and near-infrared rectified channels are given by Eqs. (3) and (4), respectively.

$$\Delta\rho_{RectRED} = \frac{\partial g_1}{\partial \rho_{BLUE}}\Delta\rho_{BLUE} + \frac{\partial g_1}{\partial \rho_{RED}}\Delta\rho_{RED} \quad (3)$$

$$\Delta\rho_{RectNIR} = \frac{\partial g_2}{\partial \rho_{BLUE}}\Delta\rho_{BLUE} + \frac{\partial g_2}{\partial \rho_{RED}}\Delta\rho_{RED} \quad (4)$$

The mathematical formula for the derivative of g_0, (polynomial formula to compute the FAPAR from the two rectified channels) with respect to the rectified red channel is given by Eq. (5)

$$\frac{\partial g_0}{\partial \rho_{RectRED}} = \frac{2(l_{04} - \rho_{RectRed})(-l_{02}\rho_{RectRed} + l_{01}\rho_{RectNIR} - l_{03})}{((l_{04} - \rho_{RectRed})^2 + (l_{05} - \rho_{RectNIR})^2 + l_{06})^2} - \frac{l_{02}}{(l_{04} - \rho_{RectRed})^2 + (l_{05} - \rho_{RectNIR})^2 + l_{06}} \quad (5)$$

and the mathematical formula for the derivative of g_0 with respect to the rectified NIR channel by Eq. (6)

$$\frac{\partial g_0}{\partial \rho_{RectNIR}} = \frac{2(l_{05} - \rho_{RectNIR})(-l_{02}\rho_{RectRed} + l_{01}\rho_{RectNIR} - l_{03})}{((l_{04} - \rho_{RectRed})^2 + (l_{05} - \rho_{RectNIR})^2 + l_{06})^2} - \frac{l_{01}}{(l_{04} - \rho_{RectRed})^2 + (l_{05} - \rho_{RectNIR})^2 + l_{06}} \quad (6)$$

The derivatives of g_n (where g_n denotes g_1 (g_2) and corresponds to the polynomial formulae to compute the rectified channel in the red (near-infrared)) with respect to the blue band, ρ_1, and with respect to the red (near-infrared) band, ρ_2, are given in Eqs. (7) and (8), respectively.

$$\frac{\partial g_n}{\partial \rho_1} = \frac{\rho_2 l_{n5} + 2l_{n1}(l_{n2} + \rho_1)}{l_{n8}(l_{n9} + \rho_2)^2 + l_{n6}(l_{n7} + \rho_1)^2 + l_{n11} + \rho_1\rho_2 l_{n10}} - \frac{(\rho_1\rho_2 l_{n5} + l_{n3}(l_{n4} + \rho_2)^2 + l_{n1}(l_{n2} + \rho_1)^2)(2l_{n6}(l_{n7} + \rho_1) + \rho_2 l_{n10})}{(l_{n8}(l_{n9} + \rho_2)^2 + l_{n6}(l_{n7} + \rho_1)^2 + l_{n11} + \rho_1\rho_2 l_{n10})^2} \quad (7)$$

$$\frac{\partial g_n}{\partial \rho_2} = \frac{\rho_1 l_{n5} + 2l_{n3}(l_{n4} + \rho_2)}{l_{n8}(l_{n9} + \rho_2)^2 + l_{n6}(l_{n7} + \rho_1)^2 + l_{n11} + \rho_1\rho_2 l_{n10}} - \frac{(\rho_1\rho_2 l_{n5} + l_{n3}(l_{n4} + \rho_2)^2 + l_{n1}(l_{n2} + \rho_1)^2)(2l_{n8}(l_{n9} + \rho_2) + \rho_1 l_{n10})}{(l_{n8}(l_{n9} + \rho_2)^2 + l_{n6}(l_{n7} + \rho_1)^2 + l_{n11} + \rho_1\rho_2 l_{n10})^2} \quad (8)$$

In Eqs (5) to (8), the notation l_{ij} corresponds to the coefficients in their intrinsic polynomial expression. The BRFs TOA simulated by the radiative transfer models, which have been used in the optimization itself, permit us to estimate the uncertainties of FAPAR using Eq. (1), as well as the expected differences between two JRC-FAPAR products derived from two different sensors as a function of their spectral band uncertainties, respectively.

2.1. Absolute accuracy of FAPAR as a function of MERIS spectral accuracies.

Figure 1 illustrates how the absolute deviations of FAPAR, ΔFAPAR, vary in the 3-D spectral space of band uncertainties. Each panel corresponds to one uncertainty value in the blue band, $\Delta\rho_{BLUE}$. The values which are mapped in the space ($\Delta\rho_{RED}$, $\Delta\rho_{NIR}$) correspond to the ΔFAPAR resulting from the average over all the simulated MERIS like data. The mean of ΔFAPAR over all the simulations increases as the spectral band uncertainties increase, mainly with the one of the blue band. Among all the results, however, large variations occur and they depend on the canopy type as well as on the atmospheric conditions and angular situations. The panels in *Figure 2* show this range of ΔFAPAR when the uncertainties of at least two bands of MERIS increase from 0 % to 10 % as function of the third band uncertainty (6 panels correspond to 6 values of uncertainty). In this section, note that $\Delta\rho_\lambda$ denotes the relative error instead of the absolute one and we used $\rho_\lambda \times \Delta\rho_\lambda$ in previous equations for computing ΔFAPAR. The top left panel, for example, illustrates how, on average, ΔFAPAR varies as function of the uncertainties of the blue band (blue color), the red band (red color) and the near-infrared band (purple color) when the two others are assumed to be 'perfect', *i.e.* with $\Delta\rho=0$. The error bar indicates the minimum and maximum values of ΔFAPAR obtained inside the training data set.

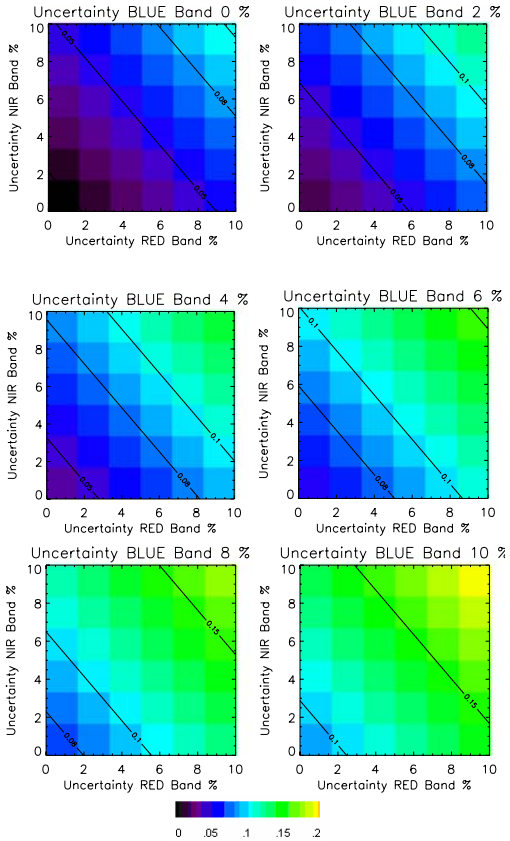

Figure 1: Average of ΔFAPAR values as function of ($\Delta\rho_{RED}$, $\Delta\rho_{NIR}$) for 6 values of $\Delta\rho_{BLUE}$.

The largest uncertainties of the three spectral bands are the largest the uncertainties in FAPAR are: this theoretically demonstrates how the calibration issues are important to assess the quality of the product.

These results shown that the average value, ΔFAPAR, can be larger than 0.1 when 2 bands have relative uncertainty values of about 4-5 %. The blue band has more impact than the red and near-infrared bands for lower values of uncertainties (*e.g.*, ΔFAPAR ≈ 0.1 if $\Delta\rho_{BLUE}$ >6 % and $\Delta\rho_{RED}$ =$\Delta\rho_{NIR}$= 2 %). This result is easily explained by the fact that we used the blue band twice in our algorithm to remove the atmospheric effects.

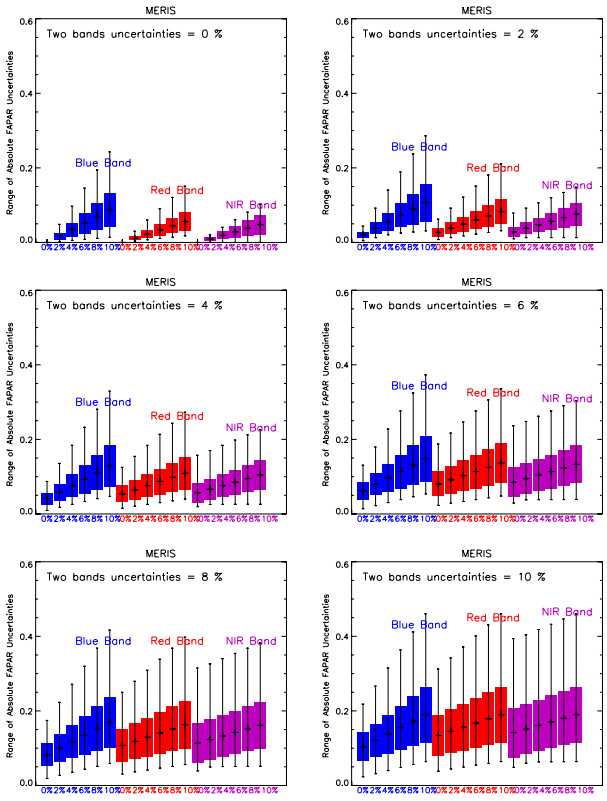

Figure 2: The 6 panels illustrate how the range of absolute deviation of FAPAR, ΔFAPAR, varies when the uncertainties of at least two bands of MERIS increase from 0% to 10 % as function of the third uncertainty band in x-axis. The cross symbol correspond to averaged value of ΔFAPAR over all simulations with the standard deviation ±σ in full column. Error bars indicate the minimum and maximum values in the ensemble.

2.2. Expected differences in FAPAR derived from SeaWiFS and MERIS as function of their blue band accuracy.

This sub-section overviews the expected impacts, when comparing the FAPAR derived from two sensors, of their respective spectral uncertainty. For example, *Figure 3* shows the scatter-plots generated when comparing the two JRC-FAPAR products derived from MERIS-like data and SeaWiFS like-data with various levels of uncertainty in the blue spectral band associated with each sensor. The data used in this plot correspond to the simulated top of atmosphere reflectances. The different colors indicate the level of uncertainties from 0 % (dark blue), 2 % (blue), 4% (light purple), 6% (orange) and 8 % (pink) in the blue band. The scattered points around the 1:1 line indicate large differences between the two FAPAR derived from the two instruments. The averaged values of the FAPAR differences between the two sensor's FAPAR products over all the synthetic cases are reported in *Figure 4* as function of the "inter-calibration" variation, represented as the difference between the two incertainties $\Delta\rho_{Blue}$(MERIS)- $\Delta\rho_{Blue}$(SeaWiFS).

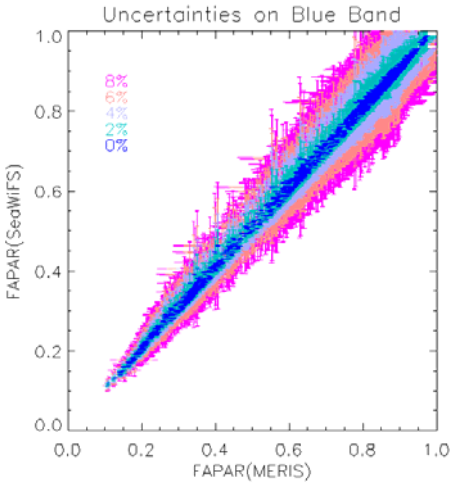

Figure 3: Comparison between FAPAR derived from SeaWiFS (y-axis) and MERIS (x-axis) in case of same geometries of illumination and observations as function of $\Delta\rho_{BLUE}$ values from 0 % to 8 %.

In this exercise, only the blue spectral band uncertainties in both instruments are taken into account. Note also that both the geometries of illumination and observation are the same when using simulated data which is not the case with actual measurements. The results in the blue band illustrate that the differences between the FAPAR derived from the two instruments increase 1) when both FAPAR values are high (see *Figure 3*) and 2) when the inter-calibration differences are higher. Other results with the red and near-infrared bands have been studied and reported in [9]. That show that the FAPAR difference increases until 0.05 when the difference 1) between the two red bands uncertainties is at about 10 %, i.e. $|\Delta\rho_{RED}(MERIS)-\Delta\rho_{RED}(SeaWiFS)| \approx 10$ % and 2) between the two NIR bands uncertainties is at about 12 %, i.e. $|\Delta\rho_{NIR}(MERIS)-\Delta\rho_{NIR}(SeaWiFS)| \approx 12$ %.

3. Comparison between FAPAR products derived from three sensors

The comparisons between FAPAR products derived from various sensors aim at assessing the performance of the physically-based algorithms which have been optimized to provide the same biophysical quantities independently of the measuring systems. Panoply of FAPAR algorithms have been developed for SeaWiFS [10] and more recently for MODIS/TERRA [11]. Preliminary comparisons between products derived from MERIS and SeaWiFS have been presented in [12] and [13] and reveal that the differences between instantaneous FAPAR values were, on average, less than 0.05.

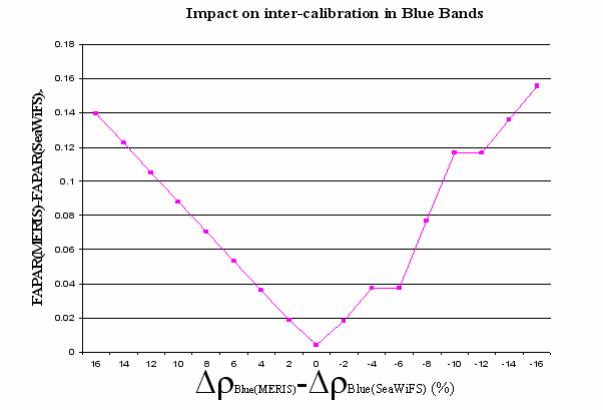

Figure 4: Averaged differences between FAPAR derived from MERIS and SeaWiFS in the case of same geometries of illumination and observations as function of the differences of uncertainties between MERIS and SeaWiFS blue bands..

Here, as an example of daily comparison of (instantaneous) FAPAR products derived from actual MERIS and MODIS data, *Figure 5* displays 2 color maps of remapped FAPAR using a color scale varying from white, green to red for the value of FAPAR about 0, 0.5 to 1.0 over the Ouagadougou region [12.15°N, 1.35ºE] on the third September 2002. The non-processed data for at least one of the two sensors have been masked (black pixels). They correspond to either shadowed, clouds contaminated or bare soil pixels. We also removed the points for which the solar (viewing) zenith angle values were higher than 60 (45) degrees. These thresholds correspond to the sun angle limit to maintain an appropriate accuracy in the atmospheric radiative transfer models and to the largest observation

angle for which the size of the pixel is larger than 2.0 km. The panels in *Figure 6* illustrate the comparison of FAPAR derived from MERIS against the FAPAR derived from MODIS. Both scatter-plot and histogram of differences are plotted using data over the vegetated pixels only, and the following statistics are reported for the differences between FAPAR values derived from the two sensors: <δ> indicates its average over all pixels, σ corresponds to its standard deviation, 'Med' is its median value and r is the linear Pearson correlation coefficient between the two data strings. The corresponding values are 0.0017, 0.0587, 0.0015 and 0.9435, respectively. A large case of comparisons over various regions have been performed and results are published in [9]: The results of the statistical values of differences are reported in Table 1.

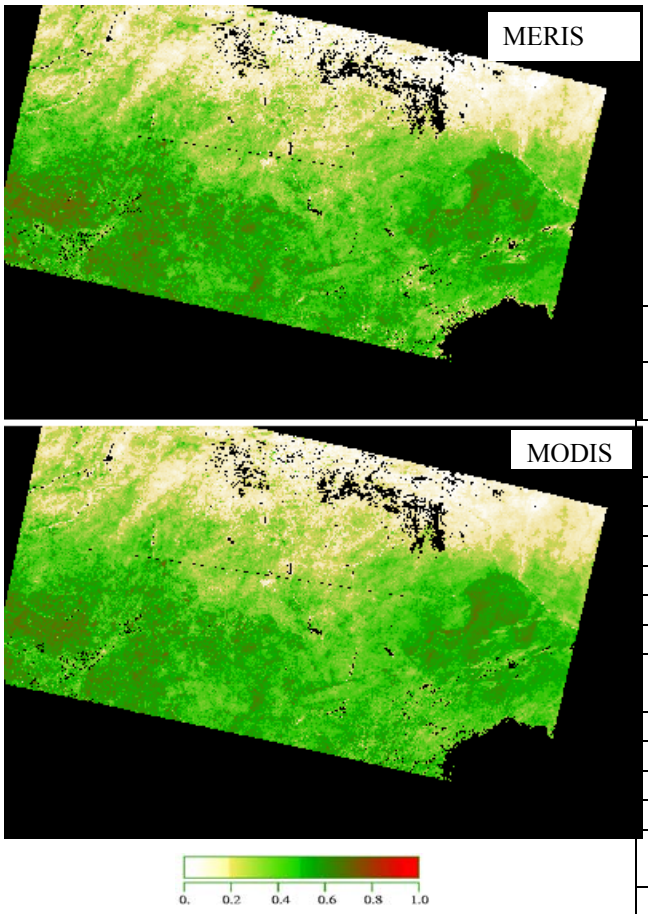

Figure 5: Maps of FAPAR values remapped at 1.2 km for MERIS and MODIS. The black pixels correspond to common mask when comparing FAPAR over Ouagadougou.

When comparing FAPAR derived from MERIS and SeaWiFS, the average value of <δ>, σ and median over all images are close to -0.02553, 0.080421 and -0.02754, respectively. The average values when comparing MERIS and MODIS are -0.04008, 0.081617 and -0.04173, respectively. Finally, when comparing SeaWiFS and MODIS, we obtain 0.00097, 0.097 and 0.00109, respectively. These last results indicate that the differences between FAPAR derived from SeaWiFS and MODIS are, in general, smallest even if the standard deviation of these differences can be much higher when comparing with FAPAR derived from MERIS.

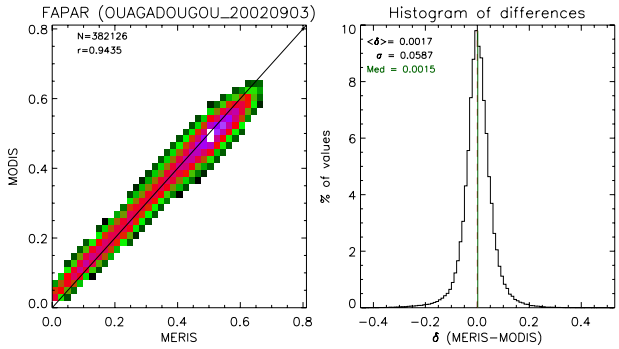

Figure 6: Scatter-plot and histogram of difference between FAPAR values remapped at 1.2 km derived from MERIS and MODIS over Ouagadougou. N indicates the number of pixels, r the correlation, <δ> the mean of differences, σ the standard deviation and med the median value of the difference.

Sensor Pair	M E R I S SeaWiFS			MERIS MODIS			SeaWiFS MODIS		
Statistics of differences	<δ>	σ	Med	<δ>	σ	Med	<δ>	σ	Med
Boreass sa	-.0158	.023	-.0168	-.0202	.0262	-0.021	-.0072	.0271	-.008
Jornada									
01/01/2003	.0103	0399	.008	.0218	.0514	0.015			
06/04/2003	-.0197	.0361	-.0213	-.0540	.0432	-0.050	-.0291	.0552	-.028
09/04/2003	-.0302	0329	-.0288	-.0086	.0315	-0.004	-.0174	.0318	-.02
10/04/2003	-.0264	0661	-.0268	-.100	.0735	-0.098	-.0322	.0723	-.02
13/04/2003	-.0239	.0578	-.0248						
Maricopa Metiolius	.0037	0448	.0066						
Yatir				.0487	.0766	-0.0450			
AAOT	-.0363	.1262	-.036	-.0502	.1163	-0.0494	-.0064	.1302	-.008
AERONET	-.0295	1208	-.0397	.0003	.0993	-0.0008	.0364	.1155	.04
BOREAS	-.0244	1197	-.0289	-.0309	.1105	-0.0311	-.0135	.1212	-.02
Geesthacht 233	-.0513	1229	-.0567	-.1181	.0659	-0.1192	.0065	.1328	.0120
Geesthacht 234	-.0514	1071	-.05	-.027	.1244	-0.0297	.0426	.1435	.036
Station_271	-.0533	1043	-.0535	-.0551	.1130	-0.0622	-.0035	.1096	-.004
Station_114	-.0092	1243	-.0168	-.0390	.1242	-0.0504	.0340	.1289	.032

Table 1: *Statistics obtained when comparing FAPAR values from three instruments over various regions.*

These comparisons have been made with daily data for which high differences in both the atmospheric and viewing conditions can partly explain the small differences, especially over regions with marked

topography. The same comparison exercise was replicated using monthly products over Europe.

The time composite algorithm applied for delivering the monthly products has been first developed for the SeaWiFS data using the framework of [14] when FAPAR products were produced using the JRC processing chain (see [15]). A new time-composite for MERIS and MODIS have been developed to take into account the diversity in the information available in the Level 2 products (*e.g.* the pixel identification see [16]).

The Level 3 products have been also remapped or aggregated into the EU-25 Lambert Azimuthal Equal Area (LAEA) projection at 2 km. *Figure 7* displays, as example, the monthly FAPAR map using a full month of MERIS data acquired in April 2003. The product has been processed at ESRIN using the Grid On Demand service (see http://eogrid.esrin.esa.int/) with the JRC codes.

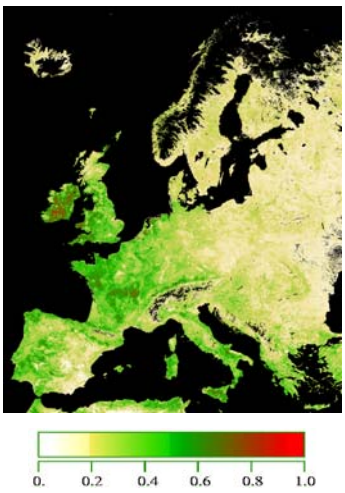

Figure 7: FAPAR map for April 2003 derived using one month of MERIS data.

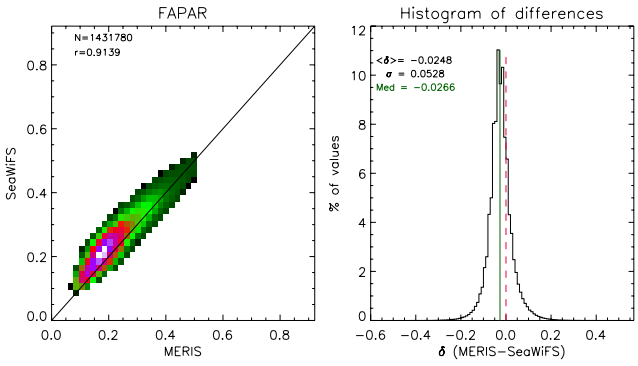

Figure 8: Scatter-plot and histogram of difference between FAPAR values remapped or aggregated at 2.0 km from SeaWiFS (y-axis) and MERIS (x-axis) over Europe in April 2003. N indicates the number of pixels, r the correlation, <δ> the mean value, σ the standard deviation and med the median value of the differences.

The results of comparisons between monthly products are shown in *Figure 8* (*Figure 9*) when comparing MERIS and SeaWiFS (MODIS). The corresponding averaged difference, <δ>, is about -0.0248 (-0.0292) with correlation coefficients close to 0.9. The reported value of FAPAR in the monthly product is the most representative value during the period and therefore may come from different date.

Scatter-plots show however a good agreement between the monthly products and the differences is in majority within the prescribed accuracy at ±0.1. They also illustrate that the time-composite technique for constructing Level-3 products enhances the consistency between three sets of FAPAR products over Europe.

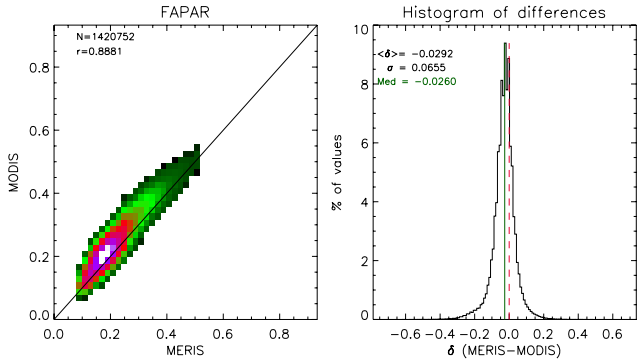

Figure 9: Same as Figure 8 but using MODIS (y-axis).

4. Comparison against ground-based estimates over one site in Senegal.

The JRC-FAPAR products derived from the SeaWiFS instrument have already been extensively compared against ground-based estimation of FAPAR over various Earth Observation System (EOS) validation sites. These sites have been categorized into various radiative transfer regimes to assess the sources of errors of the measurements and the results are published in [8]. Here, we present preliminary results with MERIS products at reduced resolution over one site, called Dahra North. The plot in *Figure 10* presents three time series (dotted symbols) of the SeaWiFS (blue color), MERIS (red color) and MODIS (orange color) FAPAR products together with the ground-based estimations (square symbols) available over this site located in Senegal [15.3675N, 15.4434E] in year 2002. Both the leaf angle distribution and Leaf Area Index have been measured by [17] for estimating the FAPAR using Eq. 9:

$$\mathrm{FAPAR} \approx 1 - \exp\left(\frac{-G(\mu_0)}{\mu_0} < \mathrm{LAI} >\right) \quad (9)$$

where $G(\mu_0)$ denotes the extinction coefficient which is computed by the Ross' function (G) as function of the

leaf angle distribution. μ_0 denotes the cosine of the solar zenith and <LAI> corresponds to the Leaf Area Index over one pixel at about a resolution of 1km. The FAPAR values are very small over this semi-arid grass savannah and signature of this vegetation phenological cycle (both for the growing and decaying periods) are remarkably well identified by both the remote sensing and ground-based estimations. Moreover, the amplitudes, both maxima and minima, are in very good agreement with each other. The daily FAPAR products derived from the three sensors agree well together and with ground estimations, again within the specified accuracy of ±0.1.

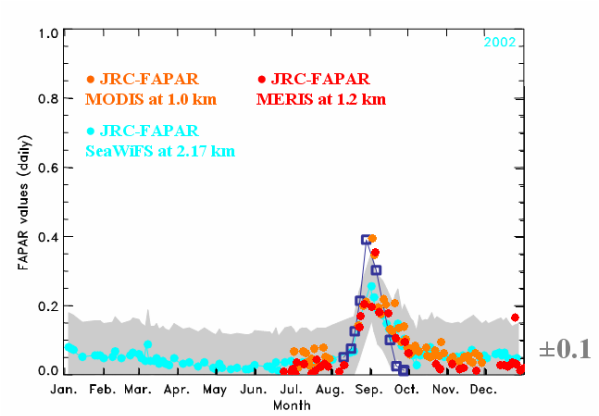

Figure 10: Comparisons of ground-based FAPAR estimates profiles (empty square symbols) and instantaneous daily SeaWiFS (blue), MODIS (orange) and MERIS (red) FAPAR products (full circle symbols) over the site of Dahra. The zone shaded in grey delineates the 0.1 uncertainty range.

5. Conclusions and perspectives

We found that there is a small bias between the FAPAR derived from MERIS (i.e. MGVI) and those derived from SeaWiFS or MODIS when comparing daily regional products. This difference is however not systematic and depends on the geographical regions selected to perform the inter-comparisons. The differences can be explained by the uncertainties at the level of radiances, since it has been shown in the first section that the differences of "inter-calibration" between SeaWiFS and MERIS can partly explain the differences on the products. At the level of monthly products (Level 3) the scatter-plots show better agreements because the outliers, that can be due to cloud and cloud shadows, have been removed and the differences are somewhat smoother. This illustrates that the time-composite technique for constructing Level-3 products enhances the consistency between the FAPAR products from various instruments. We also compared the FAPAR products against ground-based estimations over one type of vegetation and showed that the discrepancies between the three sensor products remain in the range of uncertainty expected when comparing against the ground-estimations of FAPAR.

The validation of the operational MERIS level 2 land products should continue during the life time of the instrument in order to monitor its quality which also depends on the Level 1 data. The inter-comparison was essentially conducted here with the reduced resolution data. The use of full resolution MERIS Level 2 products is also required to confirm the present results.

This type of work has also permitted us to assess the performance of the algorithm itself, different sensors provide a comparable biophysical product. The merging of the geophysical products coming from different sensors can be therefore achieved in order to provide more complete products to scientific communities regarding their spatial and temporal coverage. The time-composite technique is also very important in order to conserve the statistical distribution of daily values at various spatial and temporal resolutions.

Validation of the biophysical products is an essential task in order to provide their accuracies to the scientific communities aiming at the assimilation of remote sensing products. Comparisons with ground-based estimates and generation of global products would help to provide uncertainties associated to the spatial resolution of products. The comparison against similar products derived either from past, contemporary or future instruments would also permit us to assess any technical drift (like calibration) of sensors. However, the in-situ based estimates have to be clearly defined in term of methodology of measurements (protocol) and definition.

6. Acknowledgements

This work has been supported by the ESTEC Contract 18446/04/NL/CB. We would like to thank the SeaWiFS Project (Code 970.2) and the Distributed Active Archive Center (Code 902) at the Goddard Space Flight Center, Greenbelt, MD 20771, for the production and distribution of the SeaWiFS data, respectively. The MODIS data used in this study were acquired as part of the NASA's Earth-Sun System Division and archived and distributed by the Goddard Earth Sciences (GES) Data and Information Services Center (DISC) Distributed Active Archive Center (DAAC).

7. References

[1] GOVAERTS Y., VERSTRAETE M. M., PINTY B. AND GOBRON N. 'Designing Optimal Spectral Indices: A Feasibility and Proof of Concept Study', *International Journal of Remote Sensing*, **20**, pp. 1853-1873, 1999.

[2] GOBRON N., PINTY B., VERSTRAETE M. M. AND GOVAERTS Y. 'The MERIS Global Vegetation Index (MGVI): Description and Preliminary Application', *International Journal of Remote Sensing*, **20**, pp. 1917-1927, 1999.

[3] GOBRON N., PINTY B., VERSTRAETE M. M. AND GOVAERTS Y. 'A semi-discrete model for the scattering of light by vegetation', *Journal of Geophysical Research*, **102**, pp. 9431-9446, 1997.

[4] VERMOTE E.F., TANRÉ D., DEUZÉ J.-L., HERMAN M. AND MORCRETTE J.J. 'Second Simulation of the Satellite Signal in the Solar Spectrum: an overview', *IEEE Transactions on Geoscience and Remote Sensing*, **35**, 3, pp. 675-686, 1997.

[5] RAHMAN H., PINTY B. AND VERSTRAETE M. M. 'Coupled surface-atmosphere reflectance (CSAR) model. 2. Semi-empirical surface model usable with NOAA Advanced Very High Resolution Radiometer data', *Journal of Geophysical Research*, **98**, 20,791-20,801.

[6] GOBRON N., PINTY B., VERSTRAETE M.M, AND WIDLOWSKI J.-L. 'Advanced Vegetation Indices Optimized for Up-Coming Sensors: Design, Performance, and Applications' *IEEE Transactions on Geoscience and Remote Sensing*, **38**, pp. 2489-2505, 2000.

[7] GOBRON N., MÉLIN F., PINTY B., TABERNER M. AND VERSTRAETE M. M. 'MERIS/ENVISAT biophysical land products: Validation and performance', *Advances in Space Research*, **doi:10.1016/j.asr.2003.07.079**, 2005.

[8] GOBRON N., PINTY B., AUSSEDAT O., CHEN O., COHEN W. B., FENSHOLT R., GOND V., HUEMMRICH K. F., LAVERGNE T., MÉLIN T., PRIVETTE J. L., SANDHOLT I,. TABERNER M., TURNER D. P., VERSTRAETE M. M. AND WIDLOWSKI J.-L. 'Evaluation of FAPAR products for different canopy radiation transfer regimes: Methodology and results using JRC products derived from SeaWiFS against ground-based estimations', *Journal of Geophysical Research, in press,* 2006.

[9] GOBRON N., AUSSEDAT O., PINTY B., ROBUSTELLI M., TABERNER M., LAVERGNE T. 'Technical Assistance for the validation of the ENVISAT MGVI geophysical product. Final Report', *Institute for Environment and Sustainability*, EUR Report, In Press, 103 pp., 2006.

[10] GOBRON N., MÉLIN F., PINTY B., VERSTRAETE M. M., WIDLOWSKI J.-L. AND BUCINI G., 'A Global Vegetation Index for SeaWiFS: Design and Applications', In: Beniston M. and Verstraete M. M. (eds.)**:** *Remote Sensing and Climate Modeling: Synergies and Limitations*, pp. 5-21 Kluwer Academic, Dordrecht, 2001.

[11] GOBRON N., AUSSEDAT O., AND PINTY, B., 'MODerate Resolution Imaging Spectroradiometer (MODIS) Optimized JRC-FAPAR Algorithm - Theoretical Basis Document', *Institute for Environment and Sustainability*, EUR Report **No. 22164** EN, 19 pp., 2006.

[12] GOBRON N., TABERNER M., PINTY B., MÉLIN F., VERSTRAETE M.M. AND WIDLOWSKI J.-L. 'Evaluation of the MERIS Global Vegetation Index: Methodology and Initial Results', *Proceedings of the MERIS and ATSR Calibration and Geophysical Validation (MAVT),* Frascati, Italy, 20-23 October, 2003, European Space Agency **SP 541**, 2003.

[13] GOBRON N., MÉLIN F., PINTY B., TABERNER M. AND VERSTRAETE M. M. 'MERIS Global Vegetation Index: Evaluation and Performance', *Proceedings of the MERIS User Workshop,* Frascati, Italy, 10-14 November, European Space Agency **SP 549**, 2003.

[14] PINTY B., GOBRON N., MÉLIN F. AND VERSTRAETE M. M. 'A Time Composite Algorithm Theoretical Basis Document', *Institute for Environment and Sustainability*, EUR Report **No. 20150 EN**, 8 pp., 2002.

[15] MÉLIN F., STEINICH C., GOBRON N., PINTY B. AND VERSTRAETE M. M. 'Optimal merging of LAC and GAC data from SeaWiFS', *International Journal of Remote Sensing*, **23**, pp. 801-807, 2002.

[16] AUSSEDAT O., GOBRON N., PINTY B. AND TABERNER M. 'MERIS Level 3 Land Surface Time Composite Product Description', *Institute for Environment and Sustainability*, EUR Report **No. 22165 EN**, 17 pp., 2006.

[17] FENSHOLT R., SANDHOLT I. AND RASMUSSEN M. S., 'Evaluation of MODIS LAI, fAPAR and the relation between fAPAR and NDVI in a semi-arid environment using in situ measurements', *Remote Sensing of Environment*, **91**, 490--507, 2004.